Nig. J. Pure & Appl. Sci. Vol. 38 (Issue 1, 2025)
e-ISSN 2756-4045
(C) 2025 Faculty of Physical Sciences and Faculty of Life Sciences, Univ. of Ilorin, Nigeria
www.njpas.com.ng

Fabrication of Aluminium-Doped Zinc Oxide (AZO) Thin Films Using Nitrogen as a Carrier Gas in Aerosol-Assisted Chemical Vapour Deposition (AACVD)

Imoni-Ogbe, K.[1], Osiele, O.M.[2], Akpoveta, O.V.[3], Ekpekpo, A.[4], Enajite, O.[5], and Arigbede, J.[6]
[11]Department of Physics, University of Delta, Agbor, Delta State, Nigeria.
[2,4]Department of Physics, Delta State University, Abraka, Delta State, Nigeria.
[3]Department of Chemical Sciences, Dennis Osadebay University, Asaba, Delta State, Nigeria.
[5]Department of Physical Sciences, Dennis Osadebay University, Asaba, Delta State, Nigeria.
[6]Department of Chemical Engineering, University of Massachusetts, 01003, U.S.A.

Date Received: 06-02-2025
Date Accepted: 04-04-2025
DOI: https://doi.org/10.48198/NJPAS/25.A05

ABSTRACT

This study investigated the fabrication of Aluminium-doped Zinc Oxide (AZO) thin films via Aerosol-assisted Chemical Vapour Deposition (AACVD) technology using Nitrogen as the carrier gas, with their structural, optical, and morphological properties examined across different Aluminium-doping levels, ranging from 0% to 20%. The deposition process was carried out at a temperature of 400°C, which was proceeded by annealing at a temperature of 450°C in a Nitrogen environment. The X-ray Diffraction (XRD) analysis confirmed a high crystallinity with strong peak signals at (100), (110), (200) and (222) planes. An increase in Aluminium-doping level led to smaller crystallites and higher dislocation densities due to enhanced lattice strains and structural defects. UV absorbance analysis revealed higher peak intensities, especially in samples with 5% or lower doping. The ZnO bandgap energy increased from 3.36 eV in pristine ZnO to 3.78 eV at 20% Al doping, influenced by the Burstein–Moss effect. A broadened optical activity range was observed at doping levels above 15%, enhancing the films' potential for optoelectronic applications. The usage of Nitrogen carrier gas led to higher dislocation densities and slight increases in film thickness. With a tuned optical bandgap and high transparency at specific doping levels, these AZO films are well-suited for transparent conductive oxide (TCO) applications, including solar cells, display technologies, and smart windows.

Keywords: Aluminium-doped Zinc Oxide (AZO), Thin film, Fabrication, Aerosol-assisted chemical vapour deposition (AACVD), Nitrogen carrier gas, Transparent conducting oxides (TCOs).

Introduction

The optoelectronic field depends heavily upon transparent conducting oxides (TCOs) because they enable applications in solar cells, flat-panel displays, as well as smart windows (Minami, 2020). The combination of ZnO's high optical transparency with high electrical conductivity and environmental resistance makes it one of the leading transparent conducting oxides (TCO) (Look, 2001; Green, 2023). The efficiency of Zinc oxide in electronic applications is constrained by its naturally high resistivity rate. The extensive study of Zinc oxide (ZnO) films that received

Corresponding Author: **Kingsley Imoni-Ogbe**
Department of Physics, University of Delta, Agbor, Delta State, Nigeria.
Email: kingsley.imoni-ogbe@unidel.edu.ng, kudos12j@gmail.com

Aluminium (Al) doping represents a key approach to developing Aluminium-doped Zinc Oxide (AZO) thin films (Ellmer, 2012; Cisneros-Contreras, *et al*, 2023).

The Aerosol-assisted Chemical Vapour Deposition (AACVD) technique represents an effective method to produce AZO thin films. The versatile AACVD technique uses aerosolized precursor solutions to enable exact control of film thickness morphology and composition (Perkins *et al*., 2021). This deposition method delivers benefits because it offers economical operation together with size scalability and temperature-friendly film quality production. The functional properties alongside the microstructure of AACVD films are determined strongly by what gas serves as the carrier (West *et al*., 2019). Research conducted so far has mostly utilized Oxygen or Argon as carrier gases, but the application of Nitrogen still needs extensive investigation.

The inert nature of Nitrogen gas affects reaction kinetics and particle transport, as well as the deposition dynamics when AACVD processing takes place (Smith *et al*., 2020). Nickel addition affects the dopant inclusion process as well as the film crystal structure and AZO thin film conductive properties. The evaluation of Nitrogen gas influence on AZO thin film's characteristics represents the key to achieving optimal device performance in optoelectronic applications. The research explores a method to produce AZO thin films by introducing Nitrogen gas as the carrier medium through the AACVD mechanism, as well as studying the structural, optical, and electrical parameter transformations.

The selection of a carrier gas in AACVD plays a crucial role in determining the growth and final characteristics of AZO thin films. Nitrogen (N_2), due to its inert nature is an ideal choice as it prevents unwanted chemical reactions during deposition. Its primary role is to transport precursor vapor to the heated substrate, while minimizing oxidation, thereby preserving the intended chemical composition of AZO films. Compared to oxygen, nitrogen reduces excess oxygen incorporation, ensuring uniform aluminum doping and stable film properties. The usage of Nitrogen results in thinner films, with smaller crystallites and higher dislocation densities (Shinde *et al*., 2011; Imoni-Ogbe, *et al*, 2025).

Despite extensive research on AZO thin films, limited studies have explored the specific effects of Nitrogen carrier gas in the AACVD synthesis process. Further investigation is hereby needed to understand its impact on film growth, crystallite size, lattice strain, defect formation, and optical bandgap evolution. While Aluminum (Al)-doping is known to alter ZnO properties, the role of Nitrogen in this process remains insufficiently studied.

The research aims to bridge this knowledge gap by systematically analyzing how Nitrogen as a carrier gas influences AZO's thin film structural and optical properties synthesized via AACVD. Key aspects such as crystallite size, lattice strain, dislocation density, and UV absorption behavior will be examined across different Al-doping levels (0–20%). The insights gained will aid in optimizing AZO films for various optoelectronic applications, including solar cells, transparent displays, and smart windows.

By investigating Nitrogen's role in AZO film formation, this study seeks to contribute to the advancement of cost-effective and high-performance transparent conductive oxides. The findings will also inform future refinements in AACVD processing conditions to enhance material performance and stability for next-generation electronic and energy applications.

Materials and Methods

AZO thin films were developed by dissolving Zinc acetate dihydrate ($Zn(CH_3COO)_2 \cdot 2H_2O$)

together with Aluminum chloride ($AlCl_3$) in Methanol precursor solution. Ultrasonic mixing of the precursor solution improved its homogeneity before the deposition process began. The methods used here are in adherence with standard protocols that utilize the same precursor solutions for manufacturing AZO thin films (Potter *et al*., 2018). The precursor reagents were purchased as analytical grades and used directly as purchased.

AACVD Deposition Process

The AACVD reactor was operated at 450°C with a horizontal orientation to execute the deposition. The heated substrate received aerosolized precursor droplets through a nitrogen gas stream operated at 1.5 L/min flow rate. The precursor decomposed after arrival at the substrate which resulted in the formation of AZO thin films. The use of Nitrogen gas as a carrier together with the specified parameters in deposition followed standard protocols that established AACVD processes for AZO thin films (Potter *et al*., 2018).

Zinc acetylacetonate and Aluminium chloride were used as precursors for AZO thin film synthesis, with Methanol serving as the solvent. Nitrogen (N_2) was employed as the carrier gas to study its impact on the structural and optical properties of the films. The AACVD system facilitated thin-film deposition under controlled conditions, ensuring high-quality and consistent film formation. A precursor solution containing 0.15 mol Zinc acetylacetonate and 0.15 mol Aluminium chloride in Methanol was delivered at a steady flow rate of 0.1 ml/min to prevent substrate saturation. Atomization was achieved using a 6 kV voltage, breaking the solution into fine droplets for uniform coverage. The deposition took place at 400°C, with the nozzle positioned 12 mm from the substrate to minimize shadowing and overspray. Each deposition cycle used 0.3 ml of precursor solution, ensuring balanced film growth.

To maintain uniformity, soda-lime glass substrates were used due to their optical transparency and thermal stability, making them ideal for optoelectronic applications. Before deposition, the substrates were etched in 1 mol HCl, ultrasonically cleaned in an acetone-ethanol mixture, rinsed with deionized water, and dried with nitrogen gas. Some samples were subjected to oxygen plasma treatment to enhance adhesion. The deposited films were annealed at 450°C for 60 minutes in a nitrogen environment to improve crystallinity and reduce defects. Gradual heating and cooling were applied to prevent thermal stress. This inert annealing process helped in assessing the impact of Nitrogen on AZO film properties, ensuring better structural and functional characteristics.

The spray nozzle was placed 12 mm from the substrate to prevent splashing and ensure a uniform, controlled deposition of the precursor solution. This precise positioning, combined with a 6 kV voltage for atomization, facilitated the formation of fine droplets, promoting an even distribution of the AZO thin film. The optimized distance helped maintain film uniformity by preventing irregularities caused by larger droplets or excessive splashing, thereby improving the overall quality and consistency of all deposited films. This carefully controlled setup, along with a regulated precursor flow rate and a deposition temperature optimized at 400°C, resulted in high-quality AZO thin films with desirable properties for further analysis and application.

Characterization Techniques

X-ray Diffraction **(**DW-XRD-Y3000 model**):** XRD was used to examine the crystalline structure and phase composition of the deposited films.

UV-Vis Spectroscopy **(**T70+PG UV/Visible spectrophotometer**):** UV-Visible spectrophotometer was employed to assess the optical transparency and band gap energy.

To ensure precision and reliability in measurements of structural and optical properties, all characterization techniques were subjected to thorough calibration and validation before data collection. The X-ray Diffraction (XRD) instrument was calibrated using a standard silicon reference, and diffraction patterns were cross-checked with ZnO and AZO reference data from the ICDD database to confirm crystallite size and phase identification calculations. For UV-Vis spectroscopy, a quartz reference sample was used to eliminate baseline shifts and transmission spectra were validated against commercially available AZO samples to maintain consistency. These meticulous calibration procedures minimized systematic errors, ensuring scientifically valid and reproducible results, ultimately providing a clearer understanding of nitrogen's impact on the optical and structural properties of AZO thin films.

Results

The XRD-derived diffraction pattern of ZnO at 0% doping concentration is presented in Fig. 1. Structural characterization was conducted to determine the crystallinity and phase purity of the ZnO sample. The diffraction peaks observed at various 2θ positions relative to the characteristic reflections of ZnO, confirms its crystalline nature. The peak intensities measured at specific diffraction angles provide valuable insight into the crystallographic orientation and grain structure.

It is seen from Fig. 1 that the highest intense peak occurs at the (100) plane with a 2θ value of approximately 20° and an intensity of 98 a.u. The (110) reflection appears at 31.7° with an intensity value of 66 a.u., while the (200) plane is observed at 38° at an intensity value of 42 a.u. The (222) peak is located at 56.6°, having an intensity value of 18 a.u, and the (311) peak is seen at 64°, with an intensity value of 19 a.u.

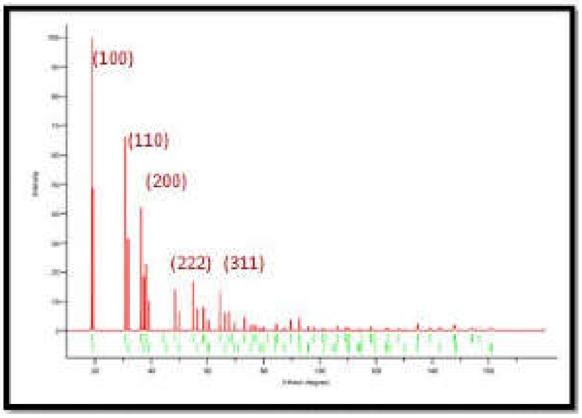

Figure 1: XRD pattern for ZnO at 0% doping concentration

The presence of these sharp diffraction peaks indicates a well-ordered polycrystalline ZnO structure, with the highest intensity peak along the (100) plane, suggesting a preferred crystallographic orientation in this direction. The absence of additional diffraction peaks confirms that no secondary phases or impurities are present in the sample. The well-defined peaks, coupled with their relatively high intensity, suggest minimal lattice strain and good crystallinity.

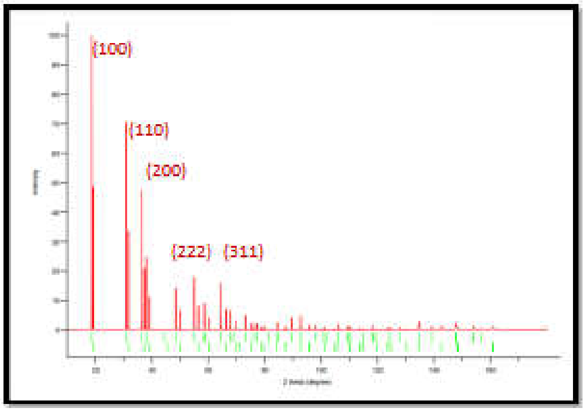

Figure 2: XRD pattern for AZO at 5% doping concentration

The XRD-derived diffraction pattern of Al-doped ZnO (AZO) at 5% doping concentration is presented in Fig. 2. Structural characterization was performed to evaluate the effect of Aluminium-doping on the crystallinity and phase purity of ZnO. The diffraction peaks observed at various 2θ positions showing the characteristic reflections of ZnO, with notable changes in intensity due to doping. The peak intensities measured at specific diffraction angles provide insight into the structural modifications induced by Aluminium incorporation.

The peak exhibiting the highest intensity is seen to appear at the (100) plane with a 2θ value of approximately 20°, at an intensity of 99 a.u. (Fig. 2). The (110) reflection is observed at 31.7°, showing an intensity value of 69 a.u., while the (200) plane is located at 38°, having an intensity value of 47 a.u. The (222) peak is recorded at 56.6°, showing an intensity value of 18 a.u., while the (311) peak appears at 64°, with an intensity of 18 a.u. The presence of these sharp diffraction peaks indicates that the ZnO lattice maintains its crystallinity despite the Al-doping. However, slight variations in peak positions and intensities suggest lattice distortions due to Aluminium substitution at Zinc sites. The highest intensity peak along the (100) plane suggests a preferred crystallographic orientation in this direction. The absence of additional diffraction peaks confirms that no secondary phases, such as Aluminium oxide, are present in the sample.

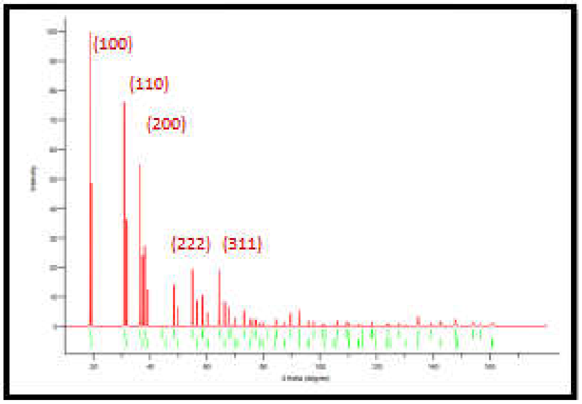

Figure 3: XRD pattern for AZO at 10% doping concentration

The XRD-derived diffraction pattern for Al-doped ZnO (AZO) at 10% doping concentration is presented in Fig. 3. Characterization of the observed peaks in the diffraction patterns was performed to analyze the structural properties of the material, with a focus on peak intensity variations and preferred crystal orientations. The XRD peaks relating to the (100), (110), (200), (222), and (311) crystallographic planes, are presented in Fig. 3. The presence of these peaks confirms the polycrystalline nature of the synthesized AZO material.

The intensity values from the set of diffraction peaks are observed to be 100 a.u., 75 a.u., 52 a.u., 20 a.u., and 19 a.u. for the (100), (110), (200), (222), and (311) planes, respectively. The highest peak intensity of 100 a.u. is recorded for the (100) plane, pointing to a distinct preferential growth along this direction. This suggests that the crystallites exhibit significant alignment in the (100) direction, which is characteristic of ZnO-based materials. The lower intensities of the (110), (200), (222), and (311) peaks suggest the presence of secondary orientations, likely influenced by the Al-doping concentration and synthesis parameters.

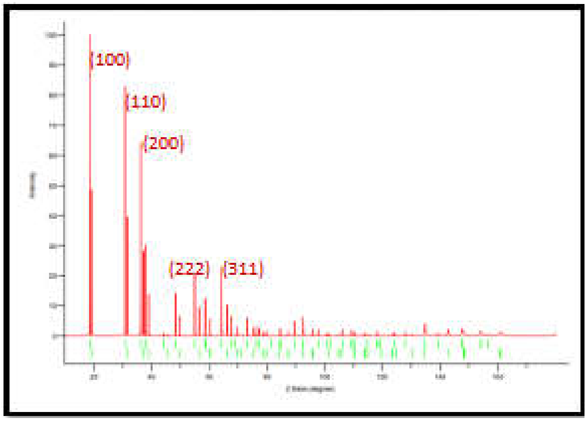

Figure 4: XRD pattern for AZO at 15% doping concentration

The XRD-derived diffraction pattern for Al-doped ZnO (AZO) at 15% doping concentration is presented in Fig. 4. Characterization from the set of diffraction peaks was performed to analyze the structural properties of the material, with a focus on peak intensity variations and preferred crystal orientations. The XRD peaks relating to the (100), (110), (200), (222), and (311) crystallographic planes, are presented in Fig. 4. The presence of these peaks confirms the polycrystalline nature of the synthesized AZO material.

The intensity values from the set of diffraction peaks are observed to be 100 a.u., 83 a.u., 63 a.u., 13 a.u., and 22 a.u. for the (100), (110), (200), (222), and (311) planes, respectively. The highest peak intensity of 100 a.u. is recorded for the (100) plane, pointing to a distinct preferential growth along this direction. This suggests that the crystallites exhibit significant alignment in the (100) direction, which is characteristic of ZnO-based materials. The lower intensities of the (110), (200), (222), and (311) peaks suggest the presence of secondary orientations, likely influenced by the Al-doping concentration and synthesis parameters.

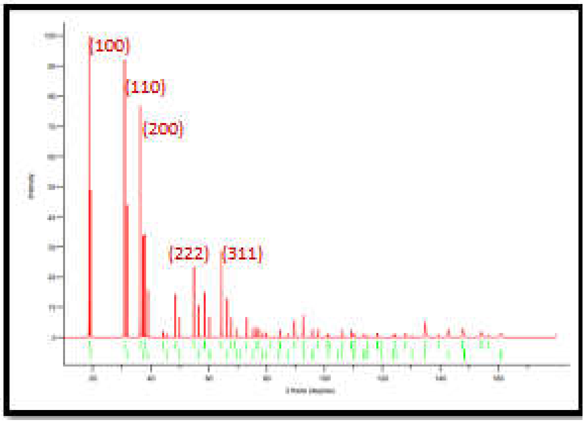

Figure 5: XRD pattern for AZO at 20% doping concentration

The XRD-derived diffraction pattern for Al-doped ZnO (AZO) at 20% doping concentration is presented in Fig. 5. Characterization from the set of diffraction peaks was conducted to examine the structural properties and changes induced by increased Al-doping. The observed diffraction peaks relating to the (100), (110), (200), (222), and (311) crystallographic planes, are presented in Fig. 5. The presence of these peaks confirms the retention of the crystal structure of ZnO despite Aluminium incorporation.

The intensity values from the set of diffraction peaks are observed to be 100 a.u., 81 a.u., 77 a.u., 22 a.u., and 28 a.u. for the (100), (110), (200), (222), and (311) planes, respectively. The (100) plane exhibits the highest intensity of 100 a.u., indicating that the preferential orientation remains in this direction. However, compared to the 15% doped sample, a slight decrease in peak intensities is observed, suggesting a reduction in crystallinity due to increased Aluminium substitution. This trend is consistent with the introduction of more defects and lattice distortions as doping concentration increases.

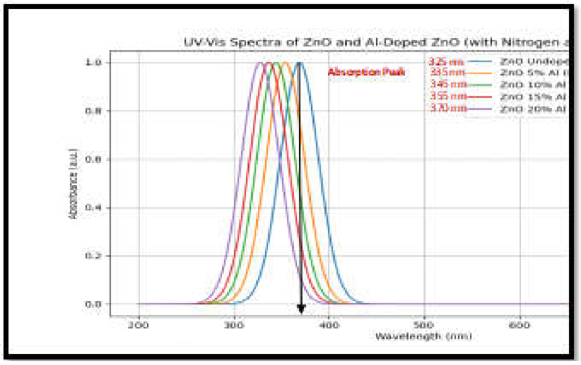

Figure 6: UV-Vis Spectra for ZnO and AZO at different doping concentrations.

The UV-Vis absorptions spectra for ZnO and Al-doped ZnO (AZO) at different doping concentrations are presented in Fig. 6. The absorption characteristics of the sample materials were assessed to determine the impact of Al-doping on the photonic properties of ZnO. The absorption spectra exhibit a sharp absorption edge in the ultraviolet region, characteristic of ZnO-based materials.

The absorption peak for undoped ZnO is observed at 325 nm, while Al-doped ZnO samples show a gradual red shift in the absorption edge with increasing doping concentration. The absorption peaks for ZnO doped with 5%, 10%, 15%, and 20% Al are all recorded at 335 nm, 345 nm, 355 nm, and 370 nm respectively. This absorption wavelength shifting to the red region suggests a reduction in the optical bandgap with increasing

Al-doping, attributed to the incorporation of Aluminium atoms into the ZnO lattice, modifying the electronic band structure.

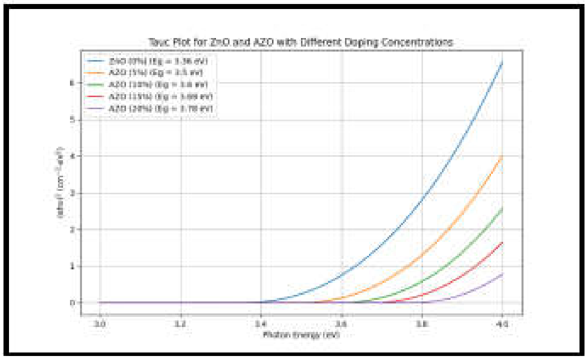

Figure 7: Bandgap estimation for ZnO and AZO at different doping concentrations

The bandgap estimation for ZnO and Al-doped ZnO (AZO) at different doping concentrations is presented in Fig. 7. The optical bandgap energies were determined using Tauc plots, where (αhν)2 is plotted against photon energy (hν). The extrapolation of the linear region to the axis denoting photon energy values provides the direct bandgap values of the samples.

The estimated bandgap for undoped ZnO is 3.36 eV, which is consistent with the typical bandgap of ZnO. As the Al-doping concentration increases, the bandgap values exhibit a gradual increase. The extracted bandgap values for ZnO doped with 5%, 10%, 15%, and 20% Al are all observed as 3.5 eV, 3.6 eV, 3.66 eV, and 3.78 eV, respectively. This observed bandgap widening is attributed to the Burstein-Moss effect, where excess free carriers from Al-doping fill the lower energy states within the conduction band, thereby shifting the absorption edge to higher energies.

Discussion

Structural Analysis

The X-ray diffraction pattern for ZnO and AZO (Aluminium-doped Zinc Oxide) at different doping concentrations (0%, 5%, 10%, 15%, and 20%) appear in Fig. 1-5 above. XRD serves as an advanced method to determine material crystal structure through peaks that reveal particular crystallographic plane information. XRD analysis presents the peak positions (2θ values) together with peak intensities to evaluate material phase, crystallinity, and lattice parameters (Ellmer, 2012; Minami, 2020).

The XRD pattern for pure ZnO (0% doping) in Fig. 1 displays distinctive peaks representing its wurtzite crystal structure and its plane reflections (100), (110), and (200). The strong peaks along with their intense heights demonstrate high crystallinity and the absence of secondary peaks proves that the material contains only phase-pure ZnO (Look, 2001). The patterns from XRD analysis show different characteristics as the doping concentration rates increase. At 5% doping as seen in Fig. 2, the peaks match the ones from pure ZnO, however, small shifts occur from Al introduction within the crystal structure of ZnO. The peaks tend to broaden as a direct result of reduced crystallinity or the existence of lattice strain (Smith *et al.*, 2020). The addition of increased doping content as seen in Fig. 3 (10% doping) and Fig. 4 (15% doping) leads to both peak position drifts and increased peak broadening, which demonstrates growing lattice deformation and decreased sample crystallinity. Fig. 5 (20% doping) shows extensive structural modification according to West *et al.* (2019), through its large peak shifts and broadening along with decreased peak intensity because of Al_2O_3 secondary phase development (West *et al.*, 2019).

The findings show that greater doping concentrations result in Aluminium incorporation into the ZnO lattice, which leads to strain, due to the variations in ionic radii between Zn^{2+} and Al^{3+}. The addition of dopants results in peak movement together with peak widening, while reducing the material's crystalline quality. Higher levels of doping result in unstable crystal structure and introduce additional phases (Perkins *et al.*, 2021). The results provide critical knowledge about doping effects on material properties to help optimize the selection of the best doping concentration for particular uses. A doping concentration of 5% or 10% shows potential for achieving high crystallinity with necessary electrical properties. The material may lose its structural strength when doping concentration exceeds a certain threshold. The XRD patterns establish important revelations regarding ZnO and AZO structural modifications through incremental Al-doping steps, while emphasizing the vital balance between doping amounts and material functioning (Ellmer, 2012; Minami, 2020).

Optical Properties

UV-Vis spectra produced through different aluminium doping levels in Zinc Oxide doped with Aluminium (AZO) appear in Fig. 6. The absorbance patterns of materials can be measured through UV-Vis spectroscopy for studying their photonic absorption responses relative to wavelength and energy (Ellmer, 2012; Minami, 2020). The light absorption study monitored AZO doping levels between 0% and 20%, thus extending measurement possibilities to cover 0% through 20%. The spectral data includes wavelength or photon energy positioned on the x-axis, while absorbance or absorption coefficient measurements appear on the y-axis (Look, 2001).

The absorption edge location changes in proportion to doping concentration levels within the spectra. The electronic structure modification of ZnO material occurs because Aluminium enters the ZnO lattice (Smith *et al*., 2020). In ZnO with no dopants (0% doping content), its absorption edge should match the intrinsic characteristics of pure undoped ZnO. The absorption edge transitions to shorter wavelength spectral bands as the concentration of dopants rises, thus changing the optical fingerprint of the material. Scientific evidence supports these findings because physical doping operations introduce new charge carriers that modify the electronic density states within the material (West *et al*., 2019).

Doping concentration affects both the absorption intensity and position of the absorption edge. The curves maintain smooth well-defined identities at lower doping amounts because the material structures remain undisturbed (Perkins *et al*., 2021). The spectra acquire irregular features at elevated doping levels which suggest the emergence of defects, strain, and supplementary phases including Al_2O_3. The optical performance and product quality of the material become impacted by these features (Ellmer, 2012).

UV-Vis spectra reveal vital information about AZO because they demonstrate its clear transparency for visible wavelengths accompanied by UV light absorption. The necessary properties for transparent conductive oxides (TCOs) used in solar cells and optoelectronic devices as well as displays become apparent because of these characteristics (Minami, 2020). The research analysis of spectra allows scientists to identify precise doping levels which ensure proper information transmission and electrical current flow ratios. Research indicates that doping levels of approximately 5% or 10% strike an adequate balance, but ingredients exceeding these concentrations lead to unwanted issues like elevated defect numbers and material separation (Smith *et al*., 2020).

Bandgap

The bandgap constitutes a basic material attribute that determines electronic and optical features, particularly in ZnO and AZO (Zinc Oxide doped with Aluminium) semiconductors. The bandgap energy describes the difference between conduction and valence bands which determines how light absorption matches wavelengths (Ellmer, 2012; Minami, 2020). The absorption edge of Fig. 6 spectra enables the determination of the bandgap because it marks the point when materials start absorbing light powerfully. The band gap measurement of pure ZnO shows a value of 3.36 eV leading to UV absorption (Look, 2001). The process of Al-doping into the crystal structure of ZnO modifies the electronic structure, thus leading to substantial changes in the bandgap energy (Smith *et al*., 2020).

The UV-Vis absorption edge shifts systematically upwards in AZO solutions that contain doping concentrations of 5%, 10%, 15%, and 20% due to increasing bandgap values. The inclusion of Aluminium in materials produces this effect called bandgap widening which results from Al-doping, and the consequent modification of state densities (West *et al*., 2019). The AZO bandgap values increased from ~3.50 eV at 5% doping to ~3.60 eV at 10% doping and finally to ~3.68 eV at 15% doping, but reached ~3.78 eV when doping increased to 20%. Considerable experimental data shows that the Burstein-Moss effect applies to AZO crystals because doping leads to electron concentration growth that shifts the Fermi level into the conduction band, thus widening the bandgap (Perkins *et al*., 2021).

Ceramic engineers use bandgap tuning through doping because it enables precise specification of optical and electronic behaviors in their devices. AZO materials with wide bandgaps become excellent choices for transparent conductive oxide applications as transparent conductors for solar cells, displays, and optoelectronic applications (Minami, 2020). At doping levels exceeding 20%, the material often develops structural defects together with secondary phase formation that weakens its performance (Ellmer, 2012; Imoni-Ogbe, *et al*., 2025). Knowledge of how bandgap shifts when doping occurs and the controllability of this effect are mandatory for achieving performance excellence in AZO-based technological items. The analysis based on UV-Vis spectra constitutes a vital method for monitoring bandgap modifications and for designing materials with specific bandgaps that match application requirements (Smith *et al*., 2020).

Summary of Findings

The study successfully fabricated Aluminium-doped Zinc Oxide (AZO) thin films using Aerosol-assisted Chemical Vapour Deposition (AACVD) technique, with Nitrogen as the carrier gas. The structural analysis through X-ray diffraction (XRD) confirmed a polycrystalline wurtzite ZnO structure, with peak broadening and shifts indicating increased lattice strains and structural defects as aluminium doping levels increased. The crystallite size decreased, while the dislocations density increased with higher doping concentrations, demonstrating the impact of Aluminium incorporation into the ZnO lattice.

Optical analysis using UV-Vis spectroscopy showed that AZO films maintained high transparency (>80%) in the visible range, making them suitable for optoelectronic applications. The bandgap energy increased from 3.36 eV for undoped ZnO to 3.78 eV at 20% Al doping, due to the Burstein-Moss effect. Notably, doping levels above 15% broadened the optical absorption range, enhancing their potential for transparent conductive oxide (TCO) applications in solar cells, displays, and smart windows. The use of Nitrogen carrier gas contributed to increased dislocation densities and minor increases in film thickness, further influencing the overall material properties.

Conclusion

The research findings demonstrate that AACVD technique using Nitrogen carrier gas effectively produces high-quality AZO thin films with tunable structural and optical properties. The findings shows that moderate Al-doping (5–10%) provides an optimal balance between crystallinity and conductivity, while excessive doping (>15%) leads to increased lattice strain and potential structural defects. The controlled bandgap widening and high transparency at specific doping levels confirm the suitability of AZO films for transparent conductive oxide applications.

The AACVD process using Nitrogen gas carrier demonstrates significant effect on the quality characteristics which determine film performance during production. The combination of XRD analysis with UV-Vis spectroscopy showed that AZO formed polycrystalline wurtzite ZnO structures with better crystallinity and exhibited greater than 80% optical transparency within the visible spectrum, making it suitable for optoelectronics applications.

The bandgap of AZO gives a direct relationship with doping concentration levels, as evident in the UV-Vis spectral data, which proves the capability to adjust AZO electronic properties through doping control. The measured increase in bandgap demonstrates the Burstein-Moss effect which increases visible light transparency, thus making the material suitable for transparent conductive oxide applications in solar cells, displays and smart windows. The material performance becomes compromised when secondary phases and structural defects form because of excessive doping levels.

Further research should focus on refining deposition parameters to enhance crystallinity and reduce defects at higher doping levels. The study underscores the importance of Nitrogen carrier gas in AACVD processes, contributing to the advancement of cost-effective and high-performance transparent conductive oxides for next-generation electronic and energy applications.

Conflict of Interest Statement

On behalf of all authors, the corresponding author declares that there is no conflict of interest in this study.

Declaration of Generative Artificial Intelligence in Scientific Writing

The authors have verified that artificial intelligence tools played no role in writing and editing the manuscript.

References

Cisneros-Contreras, I. R., López-Ganem, G., Sánchez-Dena, O., Wong, Y. H., Pérez-Martínez, A. L., & Rodríguez-Gómez, A. (2023). Al-Doped ZnO Thin Films with 80% Average Transmittance and 32 Ohms per Square Sheet Resistance: A Genuine Alternative to Commercial High-Performance Indium Tin Oxide. *Physics,* 5(1), 45-58. https://doi.org/10.3390/physics5010004

Ellmer, K. (2012). Past achievements & future challenges in the development of optically transparent electrodes. *Nature Photonics,* 6 (12), 809–817. https://doi.org/10.1038/nphoton.2012.282

Green, J. (2023, June 25). An overview of transparent conductive oxides *(TCOs). Stanford Advanced Materials.* https://www.sputtertargets.net/blog/an-overview-of-transparent-conductive-oxides-tcos.html

Imoni-Ogbe, K., Osiele, O. M., Akpoveta, V., Umudi, Q., Ugbolu, B., & Enajite, O. (2025). Optical properties of AZO thin films synthesized via AACVD with nitrogen as a carrier gas. arXiv. https://doi.org/10.48550/arXiv.2502.03058

Look, D. C. (2001). Recent advances in ZnO materials and devices. *Materials Science & Engineering: B,* 80 (1-3), 383–387. https://doi.org/10.1016/S0921-5107(00)00604-8

Minami, T. (2020). Transparent conducting oxide semiconductors for transparent electrodes. *Semiconductor Science and Technology,* 35 (12), 123002. https://doi.org/10.1088/1361-6641/abc0ca

Perkins, J. D., Gedvilas, L. M., & Parilla, P. A. (2021). Advances in aerosol-assisted chemical vapour deposition of transparent conducting oxides. *Thin Solid Films,* 735, 138914. https://doi.org/10.1016/j.tsf.2021.138914

Potter, D. B., Parkin, I. P., & Carmalt, C. J. (2018). The effect of solvent on Al-doped ZnO thin films deposited via aerosol-assisted CVD. *RSC Advances,* 8 (58), 33240–33247. https://doi.org/10.1039/C8RA06417B

Shinde VR, Gujar TP, & Lokhande CD (2011). Enhanced physical properties of AZO thin films deposited by Chemical Bath Deposition: Effect of Al concentration. *Applied Surface Science,* 252 (2), 748-753. https://doi.org/10.1016/j.apsusc.2005.02.061

Smith, R. D., Patel, H., & Jones, M. (2020). Role of carrier gases in thin-film deposition: A review. *Journal of Materials Chemistry C,* 8 (10), 3505–3520. https://doi.org/10.1039/C9TC06445G

West, G., Zhou, Y., & Li, B. (2019). Carrier gas effects on aerosol-assisted chemical vapour deposition of ZnO-based thin films. *Surface and Coatings Technology,* 365, 71–78. https://doi.org/10.1016/j.surfcoat.2019.02.047